Neuroscience 343 (2017) 398–410

ASIC CHANNEL INHIBITION ENHANCES EXCITOTOXIC NEURONAL DEATH IN AN IN VITRO MODEL OF SPINAL CORD INJURY

GRACIELA L. MAZZONE, [a]* **PRIYADHARISHINI VEERARAGHAVAN,** [b] **CARLOTA GONZALEZ-INCHAUSPE,** [c] **ANDREA NISTRI** [b,d†] **AND OSVALDO D. UCHITEL** [c†]

[a] *Laboratorios de Investigación aplicada en Neurociencias (LIAN) – Fundación para la Lucha conntra las Enfermedades Neurológicas de la Infancia (FLENI), CONICET, Buenos Aires, Argentina*

[b] *Neuroscience Department, International School for Advanced Studies (SISSA), Trieste, Italy*

[c] *Instituto de Fisiología, Biología molecular y Neurociencias, CONICET, Departamento de Fisiología, Biología Molecular y Celular, Facultad de Ciencias Exactas y Naturales, Universidad de Buenos Aires, Argentina*

[d] *Spinal Person Injury Neurorehabilitation Applied Laboratory (SPINAL), Istituto di Medicina Fisica e Riabilitazione, Udine, Italy*

Abstract—In the spinal cord high extracellular glutamate evokes excitotoxic damage with neuronal loss and severe locomotor impairment. During the cell dysfunction process, extracellular pH becomes acid and may activate acid-sensing ion channels (ASICs) which could be important contributors to neurodegenerative pathologies. Our previous studies have shown that transient application of the glutamate analog kainate (KA) evokes delayed excitotoxic death of spinal neurons, while white matter is mainly spared. The present goal was to enquire if ASIC channels modulated KA damage in relation to locomotor network function and cell death. Mouse spinal cord slices were treated with KA (0.01 or 0.1 mM) for 1 h, and then washed out for 24 h prior to analysis. RT-PCR results showed that KA (at 0.01 mM concentration that is near-threshold for damage) increased mRNA expression of ASIC1a, ASIC1b, ASIC2 and ASIC3, an effect reversed by the ASIC inhibitor 4′,6-diamidino-2-phenylindole (DAPI). A KA neurotoxic dose (0.1 mM) reduced ASIC1a and ASIC2 expression. Cell viability assays demonstrated KA-induced large damage in spinal slices from mice with ASIC1a gene ablation. Likewise, immunohistochemistry indicated significant neuronal loss when KA was followed by the ASIC inhibitors DAPI or amiloride. Electrophysiological recording from ventral roots of isolated spinal cords showed that alternating oscillatory cycles were slowed down by 0.01 mM KA, and intensely inhibited by subsequently applied DAPI or amiloride. Our data suggest that early rise in ASIC expression and function counteracted deleterious effects on spinal networks by raising the excitotoxicity threshold, a result with potential implications for improving neuroprotection.

Key words: pH, acid sensing ion channels (ASICs), neuroprotection, kainic acid, spinal cord injury, fictive locomotion.

INTRODUCTION

Spinal cord injury (SCI) is a devastating event marked by a series of cellular and molecular mechanisms that promote or contrast neuronal death and loss of locomotor activity in a process slowly developing after the primary lesion (Borgens and Liu-Snyder, 2012; Anwar et al., 2016). During this dynamic disturbance it is likely that neuronal acid homeostasis needs tight control to avoid aggravating the pathophysiological outcome (Ruffin et al., 2014). Acid pH fluctuations at synaptic (and perisynaptic) level may originate, at least in part, from the high proton content of synaptic vesicles (Sinning and Hübner, 2013) during exaggerated synaptic transmission as well as lesion-evoked neuronal disruption. Acidosis has been recently demonstrated to be a Janus-like process that may lead, on the one hand, to hyperexcitability due to dysregulation of cortical GABAergic neurons and alterations in glutamate re-uptake by astrocytes (Huang et al., 2015a), or to inhibition of glutamate receptors to curtail excessive excitation (Giffard et al., 1990; Tang et al., 1990). Furthermore, several types of voltage or ligand gated channels are modulated by pH with complex impact on neuronal excitability (Holzer, 2009), for instance activation of certain background K^+ conductances by acid pH can stabilize the resting membrane potential and depress excitability (Ma et al., 2012).

In addition to classical modulation of synaptic transmission by pH, more recent targets of protons have been identified as a subpopulation of membrane channels termed ASICs (Gründer and Pusch, 2015; Boscardin et al., 2016). ASIC channels are proton-gated, non-selective cationic channels belonging to the degenerin epithelial sodium channel superfamily

*Corresponding author. Address: LIAN-FLENI-CONICET, Ruta 9 km 52.5, B1625XAF, Belén de Escobar, Buenos Aires, Argentina.
E-mail address: mazzone@fbmc.fcen.uba.ar (G. L. Mazzone).
† Joint last authors.

Abbreviations: ANOVA, analysis of variance; ASICs, acid-sensing ion channels; AU, arbitrary unit; DAPI, 4′,6-diamidino-2-phenylindole; DIV, days in vitro; DME/HIGH, Dulbecco's modified Eagle's medium high glucose; DR, dorsal root; FCS, fetal calf serum; KA, kainate; NGF, nerve growth factor; NeuN, neuronal specific nuclear protein; PBS, phosphate-buffered saline; PI, propidium iodide; S100β, astroglial calcium-binding protein S100β; SCI, spinal cord injury; SEM, standard error of the mean; VR, ventral root.

http://dx.doi.org/10.1016/j.neuroscience.2016.12.008
0306-4522/

(Osmakov et al., 2014). ASIC channels are activated when pH falls below 7 and generate a transient inward current that rapidly fades to a shallow, persistent current potentially suitable to induce longterm effects on neurons (Alexander et al., 2011; Osmakov et al., 2014). Recent studies have proposed that activation of ASICs, particularly the ASIC1a subtype that mediates Na^+, K^+ and Ca^{2+} transmembrane flow (Yang and Palmer, 2014), plays a critical role in neuronal injury associated with neurological disorders such as brain ischemia (Krishtal, 2003), multiple sclerosis (Arun et al., 2013), and spinal cord lesion (Hu et al., 2011). Furthermore, ASIC1a channels are important mediators of aberrant plasticity of AMPA receptor-mediated synapses in the hippocampus following transient anoxia (Quintana et al., 2015). The elucidation of the acidosis mechanism involvement in acute SCI remains, however, to be clarified. Our previous studies were focused on exploiting a lesion model based on transient excitotoxic stress as the trigger mechanism for delayed damage of the spinal cord (Taccola et al., 2008; Mazzone et al., 2010; Mazzone and Nistri, 2011a). This approach stems from the notion that excitotoxicity (due to temporary, large release of glutamate) is critical for lesion amplification and severity (Oyinbo, 2011; Borgens and Liu-Snyder, 2012), and that, in a clinical setting, the associated metabolic impairment is promptly corrected with intensive care treatment (Park et al., 2004; Dietz, 2010). This model, based on the neonatal rodent isolated spinal cord and organotypic spinal slices, offers an advantageous device to test preclinical approaches to neuroprotection because excitotoxicity (evoked by the glutamate analog kainate, KA) destroys neurons with only modest white matter damage (Taccola et al., 2008; Mazzone et al., 2010; Mazzone and Nistri, 2011a). The damage is produced without intervening changes in blood pressure or general metabolism, thus providing a platform for testing proof of principle of direct neuroprotection at central level. The aim of the present study was to understand whether ASIC channel activity might have a beneficial or negative effect on the outcome of excitotoxicity studied 24 h after the primary insult and investigated with histological and electrophysiological methods. In particular, we wished to explore if modulation by ASIC channels might transform a near-threshold neurotoxic action of KA into a more damaging one in terms of histology and function.

Experiments were carried out with mouse spinal cord preparations, using wild type or ASIC1a knockout mice (Price et al., 2001; Wemmie et al., 2002), and were also performed with ASIC channel inhibitors like DAPI (Chen et al., 2010) and amiloride (Alexander et al., 2011; Leng et al., 2016) even if such drugs may exert additional effects on the nervous system.

EXPERIMENTAL PROCEDURES

Choice of spinal preparation

The present study used mouse spinal cord tissue for three preparations *in vitro*: organotypic slices, acute spinal cord slices and the isolated spinal cord. Because of the ease of accessibility and positioning of the electrochemical biosensor, the organotypic slices were used for measuring glutamate release and pH changes plus correlated tests of neuronal survival and gene expression (Mazzone and Nistri, 2011b). Acute spinal slices were employed for evaluating the local distribution of neurotoxicity assessed with fluorescence changes due to intracellular accumulation of propidium iodide (PI) in topographically-intact sub-regions and laminae to which PI could be readily distributed via bath-application. For monitoring delayed changes in neuronal survival and network activity, we used the isolated spinal cord preparation that requires several intact segments to express coordinated alternating rhythmic discharges (Kjaerulff and Kiehn, 1996) investigated electrophysiologically (Taccola et al., 2008). This approach enabled us to examine the issue of neurotoxicity from various research angles converging onto the same spinal networks (Mazzone et al., 2010; Cifra et al., 2012).

Thoracolumbar spinal cord preparations were isolated from neonatal C57BL/6J mouse (3 days old). The experiments were conducted with the approval from the Scuola Internazionale Superiore di Studi Avanzati (Trieste) Ethical Committee, in accordance with the National Institutes of Health (NIH) guidelines and the Italian act D.Lgs. 27/1/92 n. 116 (implementing the European Community directives n. 86/609 and 93/88). The experiments performed in Argentina were carried out according to National guidelines and approved by local Ethics Committees, Comisión Institucional para el Cuidado y Uso de Animales de Laboratorio (CICUAL, FCEN-UBA, act C.D. N° 3141/11, protocol N° 42). A total of 103 animals were used for the immunohistochemistry and functional analysis. Details of animal numbers in each group are as follows: sham = 19; KA = 22; KA/DAPI = 13; KA/amiloride = 27; DAPI = 9; amiloride = 13. All efforts were aimed at minimizing animal use and suffering. Spinal cords were continuously superfused in a recording chamber with Krebs' solution of the following composition (in mM): NaCl, 113; KCl, 4.5; $MgCl_2.7H_2O$, 1; $CaCl_2$, 2; NaH_2PO_4, 1; $NaHCO_3$, 25; glucose, 11; gassed with 95% O2 5% CO_2; pH 7.4 at room temperature. All details about laboratory procedures have been previously published and the experimental setup has been fully reported (Taccola et al., 2008). Drugs were dissolved in Krebs solution and bath applied at the concentrations indicated in the text.

Spinal cord organotypic slice cultures were prepared from pregnant C57BL/6J mouse, at 13 days of gestation, in accordance with our standard procedure as previously reported (Mazzone et al., 2010; Cifra et al., 2012). This study comprised 6 series of different cultures, each one yielding, on average, 40 slices for immunohistochemistry, gene expression and electrochemical release. Briefly, culture slices were grown in a medium containing 82% Dulbecco's Modified Eagle medium (DME/HIGH; osmolarity 300 mOsm, pH 7.35, "complete medium"), 8% sterile water for tissue culture, 10% fetal bovine serum (FBS Invitrogen, Carlsbad, CA, USA), 5 ng/ml nerve growth factor (NGF; Alomone Laboratories; Jerusalem, Israel), and maintained in culture for 22 days in vitro

(DIV) in accordance with standard procedures (Gahwiler, 1981; Mazzone et al., 2010). DME/HIGH, penicillin and streptomycin were purchased from Euroclone (Paignton, UK), chicken plasma was from Rockland Immunochemicals (Gilbertsville, PA, USA), thrombin was from Merck KGaA (Darmstadt, Germany). KA was purchased from Ascent Scientific (Weston-Supermare, UK). Unless otherwise indicated, other reagents were purchased from Sigma–Aldrich (Milan, Italy and Buenos Aires, Argentina).

Protocol for spinal cord excitotoxic injury

Excitotoxicity was induced by applying KA for 1 h (10 μM or 100 μM) dissolved in Krebs' solution for isolated *in vitro* spinal preparations, or complete culture medium for organotypic cultures, and then washed out to induce a minimal to moderate injury (Mazzone et al., 2010). 4′, 6-Diamidino-2-phenylindole (DAPI, Sigma–Aldrich, 3.5 μM) (Chen et al., 2010) or amiloride (Sigma–Aldrich, 100 μM) (Chen et al., 2010) was administered for 24 h after KA washout. Following KA washout, cultures were used for mRNA RT-PCR analysis, electrophysiological recordings and/or immunohistochemistry studies. Each experiment contained untreated preparations (sham) that were maintained for the same time and subjected to the same experimental procedures.

Electrochemical release

Electrochemical biosensors (Sarissa Biomedical Ltd, Coventry, UK) were used in accordance with our previous reports (Mazzone and Nistri, 2011b; Mazzone et al., 2013). On-line records were integrated with a potentiostat (Pinnacle Technology Inc., Lawrence, KS, USA) and analyzed off-line with PAL software (V1.6.7; Pinnacle Technology Inc.). Thus, we employed glutamate and null biosensors placed at each side of the ventral fissure (Fig. 1A). The current generated by released glutamate was monitored with the glutamate-sensing electrode, while the null electrode was used for recording the background current known to be directly proportional to the extracellular pH change (Llaudet et al., 2005; Robinson et al., 2008). Hence, as previously demonstrated (Llaudet et al., 2005), in control solution the null electrode current linearly grew in relation to test acidification of the medium within the 5.8–7.4 pH range (see linear plot in Fig. 1B with data fitted by the equation $y = -0.06626x + 0.486$, $R^2 = 0.9933$, $n = 6$, $p \leqslant 0.05$, t-test from 7.4 pH). Thus, a calibration curve for the null sensor was obtained using different basal solutions adjusted within the 5.8–7.4 pH range. The level of acidification detected by the null sensor was estimated as a mean current change expressed in nA. Because the experimental data were obtained from organotypic cultures whose structure normally comprises two cell layers only and, thus, they are comparatively small with respect to the extracellular volume, it seems unlikely that the calculated values reflected changes in the extracellular space. At the beginning of each experiment the specificity of the glutamate sensor was validated by using a glutamate calibration curve (0.5–50 μM) and a single point calibration (with 25 μM) was repeated at the end of each experimental day. The change of glutamate and null electrode signals were recorded simultaneously by using a basal solution (containing in mM: NaCl, 152; KCl, 5; $CaCl_2$, 2; $MgCl_2$, 1; HEPES, 10; glucose, 10, pH 7.4; 300–320 mOsm; Sigma–Aldrich, Milan, Italy).

Real-time PCR expression levels

The expression levels of ASIC1a, ASIC1b, ASIC2 and ASIC3 were evaluated in spinal cord organotypic slice cultures by real-time PCR using specific primers (Table 1). The design of primers and/or their specificity check was performed using Primer-Blast (http://www.ncbi.nlm.nih.gov/tools/primer-blast/). The total RNA was isolated using Tri Reagent solution according to the manufacture's protocol (Invitrogen). RNA samples were quantified in a spectrophotometer at 260 nm. Retrotranscription using 1 μg of total RNA was performed with an iScript cDNA Synthesis Kit (BIORAD Cat. No 170-8891) according to the manufacture's suggestions. The reaction was run in a thermocycler at 25 °C for 5 min, 42 °C for 45 min, 85 °C for 5 min. The reaction was performed in the iQ Real Time PCR Thermal Cycler (BIO-RAD) using the fluorescent dye SYBR Green (SYBR Green Supermix kit IQ™; BIO-RAD). The analysis of the results was performed using iCycle iQ Real Time PCR Detection System (BIO-RAD) program. mRNA samples were calibrated to obtain similar amplification of the 18S and β-actin as housekeeping mRNA. Cycling parameters were determined, and calculations for relative mRNA transcript levels were performed using the comparative CT method (ΔΔCT; Pfaffl, 2001) between cycle thresholds of different reactions, normalized to the housekeeping gene. Melting curve analysis was performed to assess product specificity.

Immunostaining and cell counting

Immunohistochemistry experiments were performed in accordance with previous reports (Mazzone et al., 2010; Cifra et al., 2012). Spinal cord preparations were fixed in 4% paraformaldehyde for 60 min at room temperature and stored in phosphate-buffered saline (PBS) until use or in 30% sucrose PBS for cryoprotection (24 h at 4 °C). Cryoprotective slices were cryostat-sectioned and collected sequentially on histology slides. Organotypic slices were blocked with 3% fetal calf serum (FCS), 3% bovine serum albumin (BSA), 0.3% Triton in PBS (blocking solution) for 1 h at room temperature, followed by overnight incubation at 4 °C in a blocking solution containing the previously-validated primary antibodies using the following dilutions: NeuN (1:250; Millipore, Billerica, MA, USA) and S100β (1:1000; Dako, Glostrup, Denmark). For neonatal spinal cord preparations, sections were pre-incubated in blocking solution containing with 5% FCS, 5% BSA, 0.3% Triton in PBS for 1 h at room temperature. Slices were incubated overnight at 4 °C in a solution containing 1% FCS, 1% BSA, 0.1% Triton in PBS, with primary antibodies using the following dilutions: NeuN (1:200; Millipore) and S100β (1:500; Dako). Primary antibodies were visualized using a secondary fluorescent

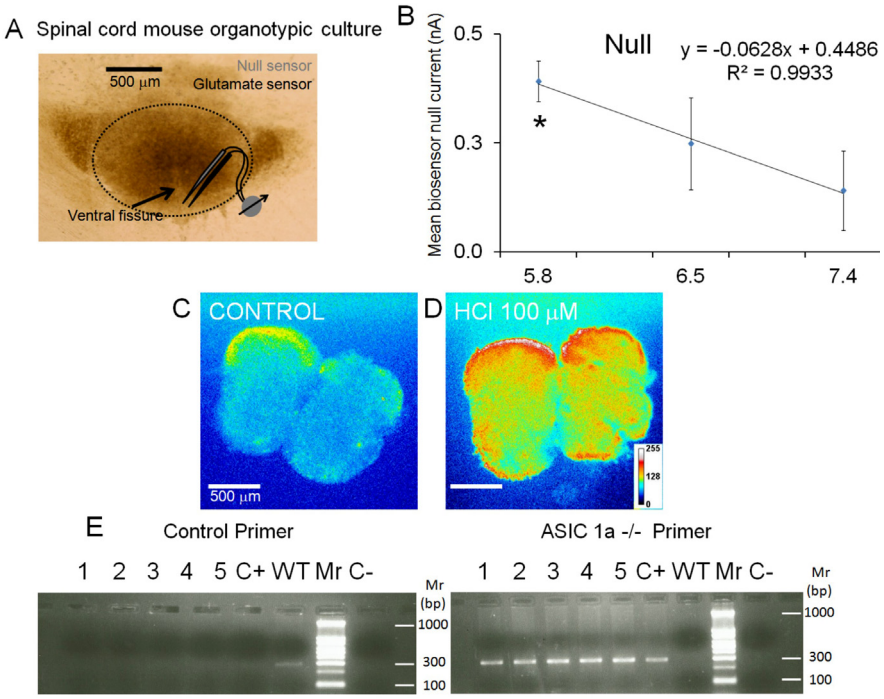

Fig. 1. pH calibration of electrochemical experiments, pH action on cell viability and gene expression by ASIC1a knockout tissue (A) Example of organotypic mouse spinal cord culture after 22 DIV showing the ventral fissure where null and glutamate sensors were placed for detection of glutamate and pH as shown in Fig. 2. (B) Calibration curve done with Krebs solution at different pH (5.8, 6.5 and 7.4) showing the mean current change for null biosensor, expressed in nA, $n = 6$, $^{*}p \leqslant 0.05$, t-test. (C, D) Examples of spinal slices stained with propidium iodide in control condition or after 5 min HCl (100 μM) application. Slices show intense propidium iodide uptake after HCl application (pseudocolor scale in D). (E) Representative experiment to demonstrate gene expression profile of wildtype or ASIC1a$^{-/-}$ spinal cord samples to validate gene ablation.

antibody (Alexa Fluor 488 or 594 at 1:500 dilution, Invitrogen, Carlsbad, CA, USA) after mounting the sections with Vectastashield medium (Vector Laboratories, Burlingame, CA, USA).

For each slice culture, the number of NeuN and S100β-positive cells was obtained by counting images with a Zeiss Axioskop2 microscope (Zeiss Axioskop2, Carl Zeiss MicroImaging, Thornwood, NY, USA) or FV300 confocal microscope (Olympus Optical, Tokyo, Japan), as previously reported (Cifra et al., 2012). The counting was performed with "eCELLence" software (Glance Vision Tech, Trieste, Italy) or by counting manually with using Image J software (version 1.49v, Wayne Rasband, National Institutes of Health, Bethesda, MD). NeuN-positive cells were counted in three regions of interest (ROIs, namely: dorsal, central and ventral). When biomarker staining was diffuse, like in the case of S100β, signals were collected as mean fluorescence intensity, expressed in arbitrary units (AU) with densitometry analysis using a Zeiss Axioskop2 microscope with MetaVue imaging software (Molecular Devices, Sunnyvale, CA) in fields of 500 × 500-μm area. For neonatal spinal cord preparations NeuN and S100β-positive cells were counted in four different ROIs: dorsal gray matter, ventral gray matter, and central gray matter (110 × 110 μm), using FV300 confocal microscope by counting stacks of 4 images (60× magnification, pinhole was airy 1 corresponding to 102 μm) in an area of 52,900 μm^2. The total number of neurons, NeuN-positive cells, and the mean fluorescence intensity for S100β astrocytes, were normalized by the ROI size (μm^2) to obtain cell density.

Propidium iodide staining

Thoracolumbar spinal cord preparations isolated from neonatal C57BL/6J mouse (3 days old), were embedded in 1.5% Agarose (Sigma)/Krebs' solution at 35 °C and allowed to solidify on ice for 5 min (Mitra and Brownstone, 2012). For these experiments, a total of 10 mice were used, 5 of them belonged to the C57BL/6J strain and 5 ASIC1a$^{-/-}$ genotype: 67 slices were obtained in total. Slice numbers used for each experimental group are as follows: C57BL/6J control = 9; KA = 13; ASIC1a$^{-/-}$ control = 9; KA = 15. Slices (300 μm) were obtained by using a vibrating tissue slicer (Integraslice 7550PSDS, Campden Instruments Limited, UK). Slices were then incubated in PEG solution (30% v/v, PEG pure in distillated water) for 60 s, and washed twice in Krebs' solution. Slices were kept in Krebs' solution (at 35 °C) gassed with 95% O_2 5% CO_2 for 1 h. After this incubation time, slices were maintained at RT for spinal cord excitotoxic injury protocol as

Table 1. List of primer sequences used for the quantification of specific mRNAs by real time RT-PCR in organotypic spinal cord cultures. The primer sequence was based on reliable amplification as previously reported (18S and ASIC1a, Baron et al., 2008; β-Actin, Mazzone et al., 2009; ASIC1b, Swain et al., 2012)

Gene	Primer Forward	Primer Reverse
β-Actin	CCTTCTTGGGTATGGAATCCTGTG	CAGCACTGTGTTGGCATAGAGG
18S	GCCGCTAGAGGTGAAATTCT	CATTCTTGGCAAATGCTTTCG
ASIC1a	GGCCAACTTCCGTAGCTTCA	ATGCCCTGCTCTGTCGTAGAA
ASIC1b	AGAATCGGAAGAAGAAGAAGAGAAG	GTAGAGCAAGTCAGGGTAGCTGAG
ASIC2a	GAGGCGCTCAATTACGAGAC	ATCATGGCTCCCTTCCTCTT
ASIC3	TGAGAGCCACCAGCTTACCT	ATGTCAAAAGTCGGACTGGG

previously described. Slices were incubated with propidium iodide staining solution (PI, P3566 – Molecular Probes, Invitrogen, Buenos Aires, Argentina, 0.2 μL/1 mL in Krebs' solution) at room temperature for 5 min in the dark. Slices were observed under a BX51WI upright microscope with a 10X objective lens (LUMPlane FI, Olympus) and an EMCCD camera (AndoriXon, Oxford Instruments), together with cell-M System Coordinator/cell-R Real Time controller software. PI quantification was done with Image J software. Fig. 1C, D shows an example of enhanced PI signal when the same spinal cord slice was treated (for 5 min) with 100 μM HCl that induced strong dye accumulation. For the present study we also used a batch of ASIC1a$^{-/-}$ mice (Wemmie et al., 2002) kindly donated by Dr. J.A. Wemmie, University of Iowa, USA. PCR tests confirmed that these mice were knockout for the ASIC1a$^{-/-}$ gene (Fig. 1E) in accordance with previous data (Price et al., 2001; Wemmie et al., 2002).

Electrophysiological recordings

Using tight-fitting Ag/Ag-Cl monopolar suction electrodes, DC–coupled records were obtained from lumbar (L2 and L5) ventral roots (VRs) that contain the motor axons of flexor–extensor motor pools of hind limbs (Taccola et al., 2008). Electrical square pulses (0.1 ms) were delivered to a single lumbar dorsal root (DR) through a bipolar suction electrode and the responses from VRs were simultaneously recorded at 10 kHz with a DP-304 Differential amplifier (Warner Instruments LLC, Hamden, CT, USA). Response threshold was determined for each preparation by applying graded electrical stimuli and detecting a minimal response in ipsilateral and ipsi-segmental VRs. Two to three times threshold stimulus intensity at frequency of 2 Hz for 15 s was given to induce DR evoked fictive locomotion (Marchetti et al., 2001). Chemically induced fictive locomotion was obtained by bath-applying N-methyl-D-aspartate (NMDA) (1.5–6 μM) plus 5-hydroxytryptamine (Kiehn and Kjaerulff, 1998) (5-HT; 10 μM). Signals were acquired and processed with pClamp software (version 9.2; Molecular Devices, Sunnyvale, CA, USA). Measurements concerning locomotor rhythm were in accordance with Taccola et al. (Taccola et al., 2008).

Statistics

Results were expressed as means ± SEM unless otherwise indicated; n refers to the number of sections (acute spinal cord slices), organotypic cultures, or isolated spinal cords. Statistical calculations were done using SigmaStat 3.11 (Systat Software, Chicago, IL, USA). To distinguish between parametric or non-parametric data, the normality test equal variance criteria were routinely used in accordance with the software directed choice. For multiple comparisons the ANOVA test for parametric data followed by the Tukey–Kramer post hoc test or Fisher's least significant difference test were used. Non-parametric values were analyzed with the Kruskal–Wallis test followed by Dunn's Method for multiple comparisons. When two groups were compared, Student's t-test for parametric data or the Mann–Whitney Rank Sum Test for non-parametric data was applied. Two groups of data were considered statistically different if $p \leqslant 0.05$.

RESULTS

Excitotoxic cell death is modulated by H^+ release

In our previous study concerned with an vitro model of SCI, we have shown that KA induces delayed excitotoxic cell death (Taccola et al., 2008) and evokes release of endogenous glutamate (Mazzone and Nistri, 2011b) with insult-related proliferation of endogenous spinal neuroprogenitors over a relatively brief time course (Mazzone et al., 2013). The early factors controlling this process and determining the functional outcome remain incompletely understood. Our previous experiments have also indicated that the release of endogenous glutamate can be quantified with a real-time electrochemical assay as a useful, simple index of spinal network activity in culture (Mazzone and Nistri, 2011b). A useful adjunct of this method is that the null electrode can be successfully

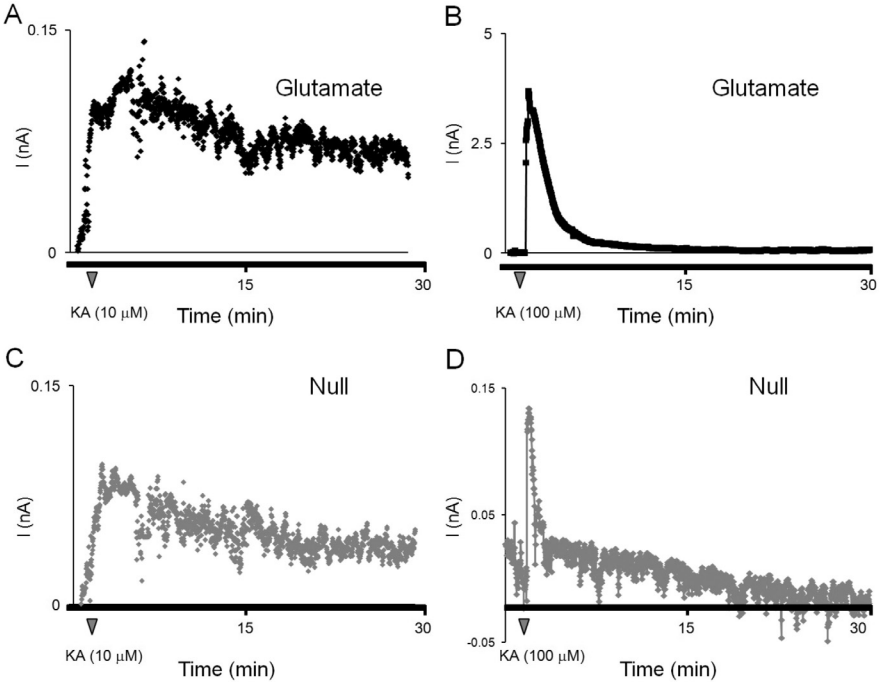

Fig. 2. Analysis of proton and glutamate release by organotypic slices with electrochemical biosensors. Average glutamate current (n = 6 slices) observed from slices exposed to KA 10 μM (**A**) or 100 μM (**B**; black traces). (C, D) the average current continuously monitored throughout the experiment with the null biosensor indicates pH changes detected with KA (10 and 100 μM). For sake of clarity, SEM values were omitted; SEM values are given for mean peak currents in the text.

employed for monitoring pH changes alongside glutamate concentrations (Llaudet et al., 2005; see Methods), thus enabling concurrent estimation of extracellular glutamate and pH. Fig. 2A, B shows average time course and extent of glutamate release induced by 10 (left) or 100 (right) μM KA from a mouse organotypic slice culture. As indicated by the different vertical scales in Fig. 2A, B, the peak amplitude of the glutamate sensor response was significantly higher with 100 than 10 μM KA (4.39 ± 1.08 vs 0.061 ± 0.004 nA, respectively, $n = 6$, $^{*}p \leqslant 0.05$, t-test): the higher gain of the latter response is accompanied by larger basal noise. For either KA concentration the signal peaked within 10 min from the start of KA application and then gradually waned to reach baseline by 30 min in analogy with former data with rat spinal slice cultures (Mazzone and Nistri, 2011b). Fig. 2C, D illustrates the concomitant changes in current recorded by the glutamate-insensitive null electrode and representing extracellular acidification. Although the response size of the null electrode was similar to the glutamate one when 10 μM KA was applied (Fig. 2C), in the presence of 100 μM KA the null electrode response peak was ten times smaller than the glutamate current signal (Fig. 2D). On the basis of the calibration plot (see Methods and Fig. 1B), it was estimated that the average pH attained during 10 μM KA application was 6.10 ± 0.09 ($n = 6$). Thus, even with a KA concentration (10 μM) that was just at threshold value to evoke excitotoxicity (Mazzone et al., 2010), the pH fall and the glutamate release peaked at the same time (2.7 ± 0.7 or 2.7 ± 0.6 min for pH or glutamate, respectively ($n = 5$, p = 0.926, t-test) with a similar rate of rise (τ value = 0.8 ± 0.4 or 0.5 ± 0.4 min, respectively; $n = 5$, p = 0.166, t-test). These observations suggested that these two parameters were likely interconnected, a notion compatible with the view that protons perhaps released by spinal cells might act as neuromodulators (Ruffin et al., 2014).

To further evaluate how pH changes might impact on the extent and topography of early cell damage induced by KA, we studied the topographical distribution of the fluorescent probe PI that, being a large molecule, readily accumulates inside cells with damaged plasma membrane (Brana et al., 2002). Fig. 3A shows examples of PI fluorescence signals in spinal cord slices treated with KA (10 μM; 1 h) (Fig. 3B) that, at this concentration, yielded minimal cell death (Fig. 3B) in accordance with the modest release of glutamate (Fig. 2A). Further observations suggested that this phenomenon was related to extracellular pH and the ability to activate ASIC channels. In fact, Fig. 3C, E, F compares the PI signals from WT and ASIC1a$^{-/-}$ spinal slices, indicating that, in this genotype, the toxic effect of KA was intensified (n = 9–15 slices, $^{*}p \leqslant 0.05$, t-test, vs. control). These data unexpectedly suggested that extracellular protons could exert some damage-limiting action against excitotoxicity.

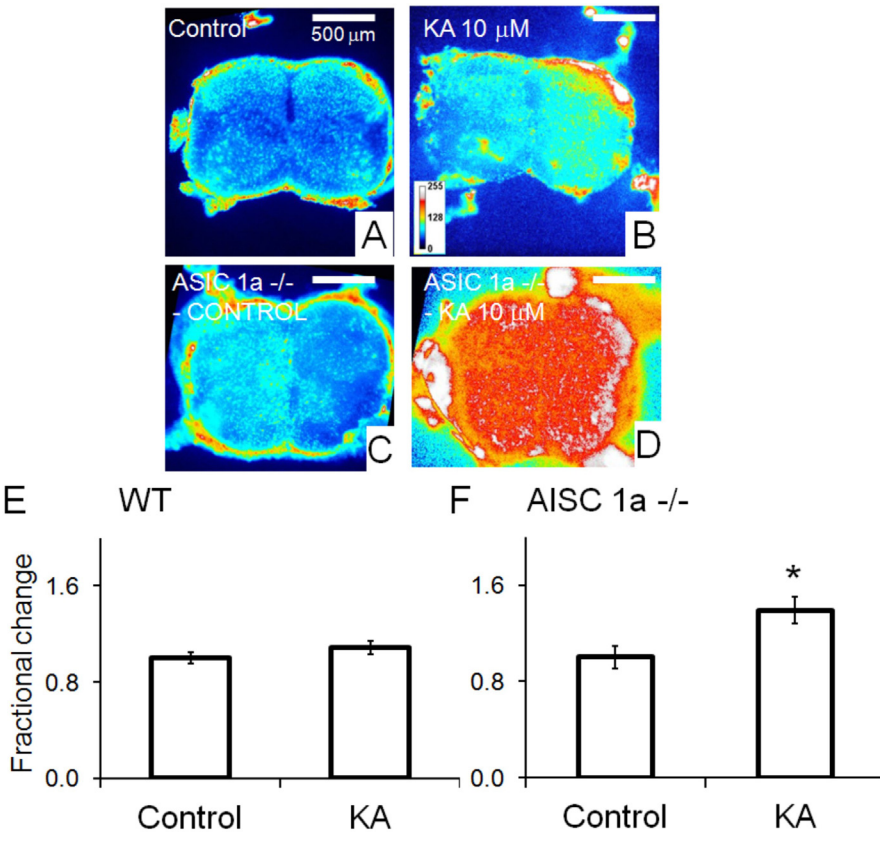

Fig. 3. Analysis of cell death induced by KA using propidium iodide staining of spinal slices. Cross sections of spinal slices (A-D) in control condition or after 1 h KA (10 μM) application for WT animals or ASIC1a$^{-/-}$. Signals are coded by pseudocolors. (E, F) Histograms comparing the effect of KA on WT and ASIC1a$^{-/-}$ slices: data are expressed as fractional change in average propidium iodide fluorescence intensity over control; n = 9–15 slices from 8 independent experiments, $^{*}p \leqslant 0.05$, t-test, vs. control.

ASIC channel mRNA modulation induced by KA

We next investigated whether KA mediated excitotoxicity might impact on the expression of ASIC1a, 1b, 2 and 3 by spinal cord organotypic cultures evaluated by RT-PCR. ASIC1a and ASIC2 are specific for spinal cord tissue, while ASIC1b and 3 are expressed by other structures like DRGs and non-neuronal cells (Deval and Lingueglia, 2015). In preliminary experiments we validated (by quantitative RT-PCR) the ASIC gene expression in spinal cord organotypic cultures. As described in previous studies (Baron et al., 2008), ASIC1a and ASIC2 were the predominant mRNAs in these preparations (1.26 ± 0.01 and 1.10 ± 0.06 change over the house keeping gene products β-actin and 18S, $n = 3$ experiments), whereas ASIC3 and ASIC1b expression was relatively low (0.89 ± 0.15 and 0.63 ± 0.08,

$n = 3$) consistent with their specific location to sensory neurons (Deval and Lingueglia, 2015) and ciliated neurons of the spinal cord central canal (Jalalvand et al., 2016b).

In the current experiments on organotypic slices treated with KA (1 h) and analyzed 24 h later, the mRNA level of all four ASIC genes was significantly upregulated by 10 μM KA, while, on the contrary, only ASIC1a and ASIC2 were significantly reduced by KA (100 μM; Fig. 4, $n = 15$ slices for each experimental condition from 3 independent experiments; $^{**}p \leqslant 0.01$, $^{*}p \leqslant 0.05$ vs control; Kruskal–Wallis, Dunn's Method) in line with the large toxicity evoked by such a high KA concentration (Mazzone et al., 2010). Unexpectedly, when slices were incubated with DAPI, a previously reported ASIC inhibitor (Chen et al., 2010; Alexander et al., 2011), for 24 h during KA washout, the upregulation of ASIC1a, ASIC1b and ASIC 3 was prevented (Fig. 4, $n = 15$ slices for each experimental condition from 3 independent experiments; $^{\#}p \leqslant 0.05$, $^{\#\#}p \leqslant 0.01$ vs KA 10 μM, Kruskal–Wallis, Dunn's Method). DAPI alone had no effect on any ASIC gene expression.

Cell loss mediated by ASIC inhibitors

Representative images of NeuN (neuron)- and S100β (glial)-positive cells in spinal cord organotypic culture treated with KA (10 μM) followed by 24 h DAPI application are shown in Fig. 5A. These data indicate that no toxic effect was apparent 24 h after washout of KA (Fig. 5A, B, C). Conversely, histograms show that the number of neurons and glial cells fell 24 h after KA application plus DAPI (Fig. 4A, B and C, respectively). While neuron numbers were unaffected by DAPI alone for 24 h, the average fluorescence signal from glia was significantly lowered after DAPI ($n = 11$–22 slices, $^{*}p \leqslant 0.05$ vs control, $^{\#}p \leqslant 0.05$ vs KA, Kruskal–Wallis, Dunn's Method) in accordance with the report of its potentially toxic effect on proliferative cells via inhibition of RNA and DNA polymerase (Baraldi et al., 2004).

We next compared two ASIC inhibitors, namely DAPI and amiloride (AM, 100 μM), for their effect on KA neurotoxicity in the isolated mouse spinal cord 24 h later (Fig. 6). Fig. 6A shows representative images of regions of interest (ROIs) in spinal cord sections under control condition, after KA treatment only, or after KA application followed by DAPI or amiloride. Fig. 6A shows that, in the three ROIs examined 24 h after KA (10 μM; 1 h application), neuronal survival was excellent to confirm the lack of neurotoxicity of this low concentration of the glutamate agonist (Table 2). When DAPI or amiloride were administered for 24 h after KA washout, neuronal numbers were significantly decreased (Fig. 6C, D and Fig. 6B, respectively) as exemplified by quantification for the central ROI (Fig. 6E, $n = 9$–29, $^{*}p \leqslant 0.05$ vs control, $^{\#}p \leqslant 0.05$ vs AM alone, Kruskal–Wallis, Dunn's Method, $^{\$}p \leqslant 0.005$ vs DAPI alone, Mann–Whitney Rank Sum Test) which is the one believed to contain the central pattern generator for locomotion (Kiehn, 2006, 2016). The insets to Fig. 6D indicate that DAPI administration after KA was associated

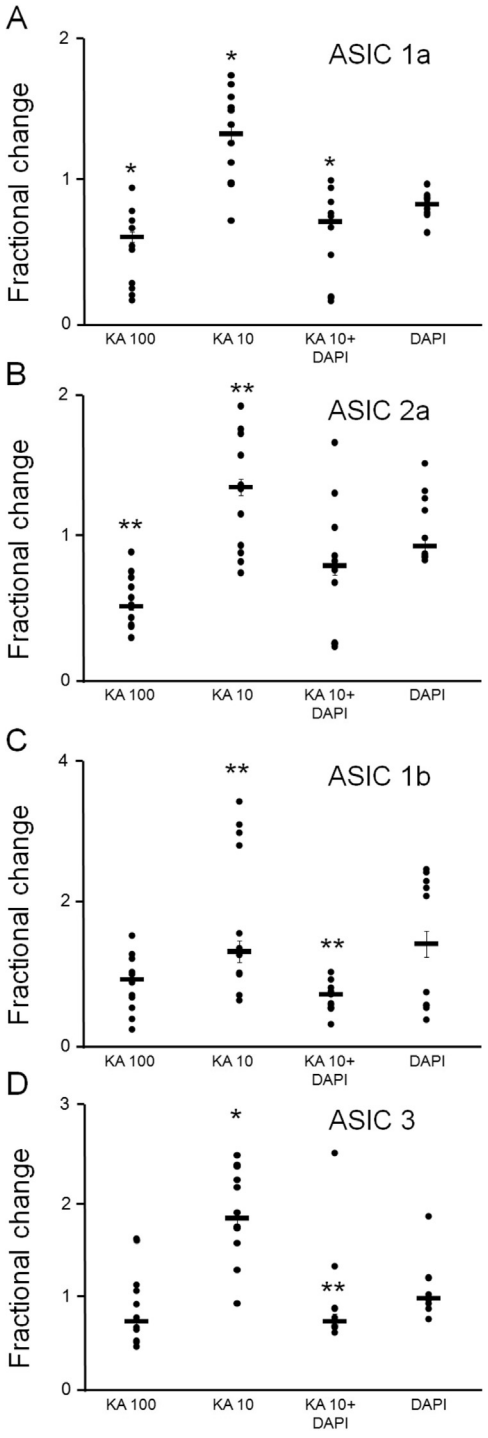

Fig. 4. ASIC mRNA expression in organotypic spinal cord cultures by RT-PCR. Ordinate: fractional change with respect to control condition. Cultures treated with KA (10 μM and 100 μM) demonstrated changes in the levels of mRNA transcripts of ASIC1a (A), ASIC1b (B), ASIC2a (C), ASIC3 (D). mRNA increase was significant reduced by addition of DAPI (3.5 μM) during KA (10 μM) washout. For each ASIC gene product, amplification values were normalized with β-actin and 18S mRNA levels. Control level was set at 1 for each gene product; medians (black horizontal line) and individual data (filled circles) are shown in each panel, $n = 15$. Different slices for each experimental condition from 3 independent experiments. For each ASIC gene, $^{*}p \leqslant 0.05$, $^{**}p \leqslant 0.01$, vs control; $^{\#}p \leqslant 0.05$, $^{\#\#}p \leqslant 0.01$, vs KA10 μM, Kruskal–Wallis, Dunn's Method).

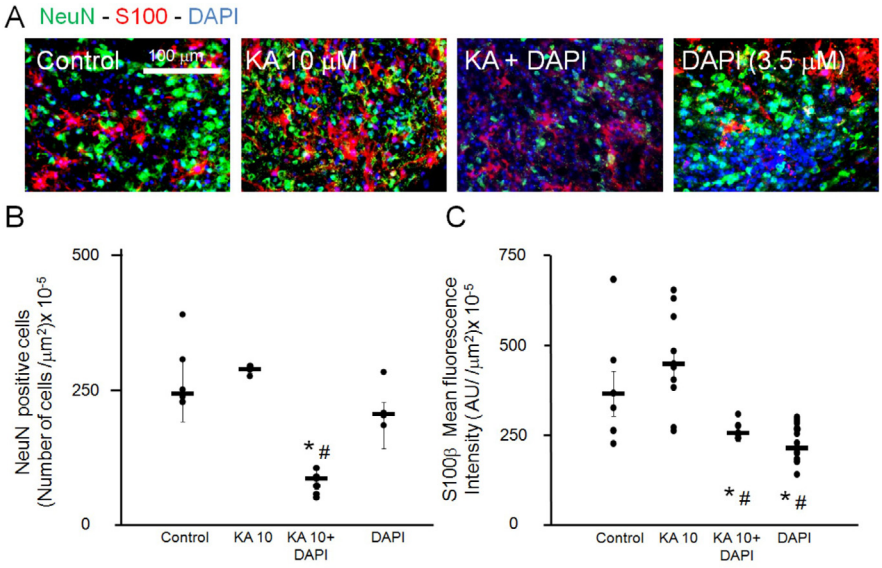

Fig. 5. Quantification of neuronal and glial staining in organotypic spinal cord cultures. (A) Example of neuronal and glial staining in control condition (NeuN red, S100β green, DAPI blue) in spinal cord organotypic cultures. (B) Plots show the median of NeuN-positive cells (black horizontal line) calculated 24 h after the application of KA (10 μM; 1 h) in control or DAPI (3.5 μM) solution, and the distribution of individual data (filled circles), $n = 4–7$ slices, $^{*}p \leqslant 0.05$ vs control, $^{\#}p \leqslant 0.05$ vs KA, Kruskal–Wallis, Dunn's Method. (C) Plots show the median of fluorescent intensity data (arbitrary units, black horizontal line) together with the distribution of single measurements for S100β antibody signal detected at 24 h, $n = 11–22$ slices, $^{*}p \leqslant 0.05$ vs control, $^{\#}p \leqslant 0.05$ vs KA, Kruskal–Wallis, Dunn's Method.

with pyknosis shown as condensed chromatin appearance (Taccola et al., 2008; Mazzone et al., 2010). No change in S100β-positive astrocytes was observed (Fig. 6A-D). It is noteworthy that neither amiloride nor DAPI applied alone induced significant neuronal loss (Fig. 6C–E).

It should be noted that there was an apparent discrepancy in the strength of the effects of 10 μM KA followed by DAPI on cell survival (Fig. 5B for organotypic slices and Fig. 6E for isolated spinal cords): we propose that the simpler bilayered structure of the organotypic slice (Cifra et al., 2012) with comparatively fewer glial cells might have been less efficiently equipped to handle glutamate release and pH changes. Our data, thus, suggested that, regardless the type of ASIC inhibitor used, their application converted a near-threshold excitotoxic stimulus to a neurotoxic one.

ASIC inhibitors enhanced functional disruption by excitotoxicity

We next evaluated the effect of 10 μM KA, DAPI or amiloride (either applied alone or in combination) on synaptic transmission in the isolated spinal cord. Amiloride alone depressed the polysynaptic peak amplitude and made significant decrease on mono and polysynaptic transmission following KA application (Table 3). In addition to testing synaptic activity evoked by single pulses applied to one DR, we also investigated the coherent expression of rhythmic network discharges expressed as fictive locomotion evoked by DR stimulus trains (Marchetti et al., 2001) and emerging as regular bouts of oscillations alternating among ventral roots (VRs; Fig. 7). This phenomenon comprises a slowly developing cumulative depolarization caused by nonlinear summation of synaptic inputs (Sivilotti et al., 1993; Baranauskas and Nistri, 1996; Barbieri and Nistri, 2001) with superimposed spiking and oscillatory cycles, none of which was affected by subthreshold concentration of KA (10 μM; Fig. 7A-D). Nevertheless, KA treatment followed by DAPI or amiloride for 24 h elicited significant decrease in the number of oscillations (Fig. 7B). Significant depression of cumulative depolarization by amiloride applied after KA was also observed (Fig. 7C, D).

Alternating rhythmic oscillations recorded from lumbar VRs are thought to indicate the functional output of the locomotor central pattern generator (Kiehn, 2006, 2016). In the present experiments, NMDA (1.5–6 μM) plus 5HT (10 μM; see Methods) were used to generate such oscillations (Beato et al., 1997). Despite using a range of NMDA doses, oscillations expressed by mouse preparations are less stable and persistent than in other mammalian species (Zhong et al., 2012) as confirmed in our tests: this characteristic was present even after 24 h in vitro in the present experiments. In fact, only 3/11 spinal cords generated 20 consecutive cycles rhythmically alternating among flexor and extensor motor pools used a standard index of fictive locomotion (Kjaerulff and Kiehn, 1996) and exemplified in Fig. 8. These cycles were all expressed at low periodicity (10.3 ± 3.6 s; $n = 6$). The remaining preparations generated variable bouts of alternating rhythmic discharges (4 to 12). After exposure to KA (10 μM), the probability of observing 20 cycles remained similarly low (2/12 preparations), and the number of cycles in a bout varied from 4 to 12 (in 4/12 preparations) with average period of 14.6 ± 2.3 s ($n = 6$) and lacking alternation. DAPI or amiloride did not significantly change these patterns when they were applied after KA (2/5 or 8/12 spinal cords for DAPI or amiloride, respectively) while cycle periodicity remained slow (14.0 ± 1.6 or 17.8 ± 2.1 s, respectively). Cycle alternation was preserved with DAPI or amiloride per se, yet absent when these drugs followed KA.

These results could not be simply attributed to inefficient network depolarization by NMDA and 5HT because the average VR depolarization evoked by 3 μM NMDA and 10 μM 5-HT was similar in sham (0.72 ± 0.08 mV, $n = 11$), after KA (0.64 ± 0.07 mV, $n = 12$), DAPI (0.95 ± 0.19 mV, $n = 7$) or amiloride (0.55 ± 0.14 mV, $n = 5$) protocols, even when applied after KA (0.47 ± 0.06 or 0.49 ± 0.08 mV, $n = 5$ or $n = 12$, respectively).

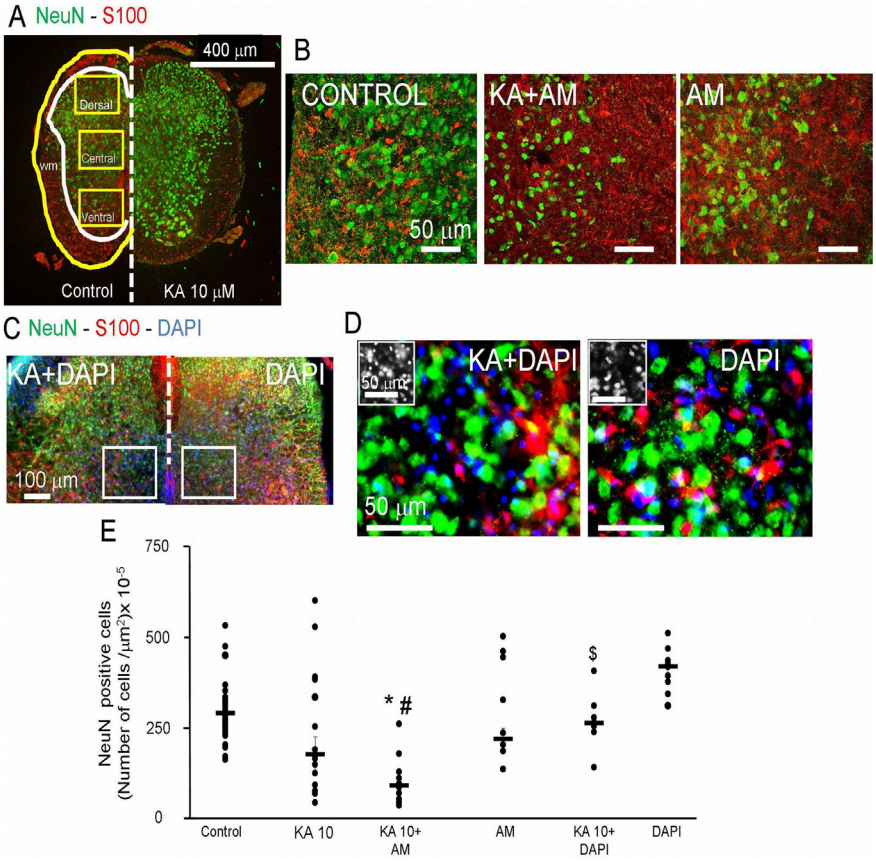

Fig. 6. Neuronal and glial staining of mouse isolated spinal cord. (A) The upper left panel shows an example of neuronal and glial staining (NeuN green, S100β red) in mouse isolated spinal cord in control condition (left) or 24 h after the application of KA (10 μM) for 1 h (right). Three different gray matter ROIs, namely dorsal, central and ventral, are delimited by yellow boxes. (B) Example of neuronal and glial staining in control condition or 24 h after the application of KA (10 μM) followed by amiloride (AM, 100 μM) or amiloride only. (C, D) Examples of NeuN and S100β staining (low or high magnification, respectively) after the application of KA (10 μM) followed by DAPI (3.5 μM) or DAPI per se. Insets in panels D shows the condensed chromatin nucleus as marker for pyknosis. (E) Plots show the median of NeuN-positive cells (black horizontal line) in the central area for control condition and 24 h after the application of KA (10 μM, 1 h) alone or followed by amiloride (AM, 100 μM) or DAPI (3.5 μM), and the distribution of individual data points (filled circles); n = 9–29 slices, 6 independent experiments were done to include in each case 2–8 spinal cords, $^{*}p \leqslant 0.05$ vs control, $^{\#}p \leqslant 0.05$ vs AM alone, Kruskal–Wallis, Dunn's Method; $^{\$}p \leqslant 0.005$ vs DAPI alone, Mann–Whitney Rank Sum Test.

Table 2. Quantification of NeuN-positive neurons in three ROIs

ROIs	Sham	24 h after KA
Dorsal	312.5 ± 26.1	373.9 ± 46.8
Central	324.4 ± 18.5	222.2 ± 47.9
Ventral	280.2 ± 32.5	245.3 ± 32.7

Data are mean ± s.e.m. from 3 independent experiments, in each one n = 6–7 lumbar sections were analyzed and their data were averaged.

DISCUSSION

The present report shows that, in mouse spinal cord networks, the histological and functional outcome of excitotoxicity could depend on extracellular pH changes that likely involved activation of ASIC channels, and were important for the operation of locomotor circuitry. It was unexpected that inhibitors of ASIC channels or ASIC1a genetic ablation actually intensified the damage evoked by a borderline excitotoxic stimulus.

Protons modulate neurotoxicity

Notwithstanding the multifarious effects of acidification on neuronal receptors and channels (Holzer, 2009), the role of ASICs in the central nervous system is complex and subjected to intense regulation to modulate and transmit network signals (Krishtal, 2003) related to pathological and physiological conditions (Duan et al., 2007; Baron et al., 2008). For instance, during brain ischemia affecting mouse cortical neurons, the activation of homomeric ASIC1a channels (highly permeant to Ca^{2+}) may play a key role in acidosis-induced neuronal death (Xiong et al., 2004). Decreases in extracellular pH to 6.5 (or below) occur in several pathologies such as cerebral ischemia, hypoxia or epilepsy due to increased lactate production by glycolysis, and, moreover, even sustained neuronal activity can lower pH (Chu and Xiong, 2012). In physiological conditions transient acidosis is normally compensated by proton uptake, for instance during glutamate release (Hnasko and Edwards, 2012). Buffering H^+ to keep the intracellular neuronal pH around 7.1 is effected by membrane located acid-base transporters (Chesler, 2003).

While the extracellular pH value is normally 7.4, intense, sustained transmitter release (when synaptic vesicles with internal pH of ~5.5 discharge their content) can significantly acidify the synaptic cleft (Hnasko and Edwards, 2012). It follows that using KA to persistently stimulate release of glutamate stored in synaptic vesicles is likely to provide, within spinal networks, a microenvironment with acid pH to which glia might have also contributed. In fact, stimulation of astrocytes from neonate mouse brain cortex acidifies the extracellular space leading to activation of neuronal ASIC1a channels and firing of action potentials (Li et al., 2014). This finding implies a functional interaction between neurons and astrocytes for proton regulation, a process that perhaps was operative in spinal networks as well.

In the present study extracellular acidification by KA was evaluated with simultaneous recording via the glutamate biosensor and the null electrode as recently demonstrated (Llaudet et al., 2005). Although the background current attributed to pH changes faded away during KA application, we first suspected that the early fall in extracellular pH might have triggered the activation of

Table 3. Effects of KA, amiloride or DAPI on synaptic transmission

Reflex Parameters	Sham (n = 11)	KA(10 μM; 1 h; n = 14)	KA(1 h)/ DAPI (3.5 μM; 24 h; n = 11)	DAPI (3.5 μM; 24 h; n = 7)	KA(1 h)/AMILORIDE (100 μM; 24 h; n = 16)	AMILORIDE (100 μM; 24 h; n = 7)
Monosynaptic amplitude (mV)	0.04 ± 0.01	0.04 ± 0.02	0.04 ± 0.01	0.05 ± 0.01	0.04 ± 0.01	0.03 ± 0.01
Monosynaptic Area (mV.ms)	7.47 ± 1.98	6.39 ± 1.46	6.19 ± 2.01	8.48 ± 1.11	**3.23 ± 0.33***	5.90 ± 1.51
Polysynaptic amplitude (mV)	0.41 ± 0.09	0.40 ± 0.06	0.32 ± 0.08	0.32 ± 0.10	**0.20 ± 0.03***	**0.18 ± 0.02***
Polysynaptic area (mV.ms)	1892.90 ± 803.39	1888.57 ± 507.25	1109.58 ± 200.91	1357.94 ± 398.65	1323.21 ± 204.94	2145.08 ± 350.69

* $P < 0.05$ vs sham data.

deleterious processes that were then translated into neuronal cell death (Shabbir et al., 2015a). To our surprise, we observed that, while no significant increase in cell death was evoked by 10 μM KA as previously reported (Mazzone et al., 2010), the borderline between survival and death was readily surpassed in the presence of two different ASIC inhibitors, namely DAPI or amiloride, or with genetic ablation of the ASIC1a gene. Finally, upregulation of ASIC mRNA was observed after KA application. Altogether, these data unexpectedly indicated that a fall in extracellular pH induced by KA was somehow protecting from cell death.

ASIC expression in spinal networks

Functional ASICs are homo or heterotrimers of different subunit assembly. To date, six subunits of ASICs have been identified, namely 1a, 1b, 2a, 2b, 3, and 4 (Krishtal, 2003). Our data suggest a predominant role for the ASIC1a and ASIC2a subunits in response to KA in mouse spinal networks in analogy with previous studies (Deval and Lingueglia, 2015). A former investigation has shown that ASIC1 and 2 subtypes are expressed by the majority of small as well as large neurons in all laminae of the spinal cord (Baron et al., 2008).When 100 μM KA induced extensive neuronal cell death without large glial loss (Mazzone et al., 2010), significant reduction in ASIC1a and ASIC2 occurred attributable to cell loss. On the contrary, when 10 μM KA was applied, significant mRNA increase was observed for all subunits. To further investigate the contribution by ASICs to excitotoxicity following KA administration, DAPI, a potent ASIC inhibitor (Chen et al., 2010), was applied during the KA washout and observed to decrease mRNA expression of all subunits.

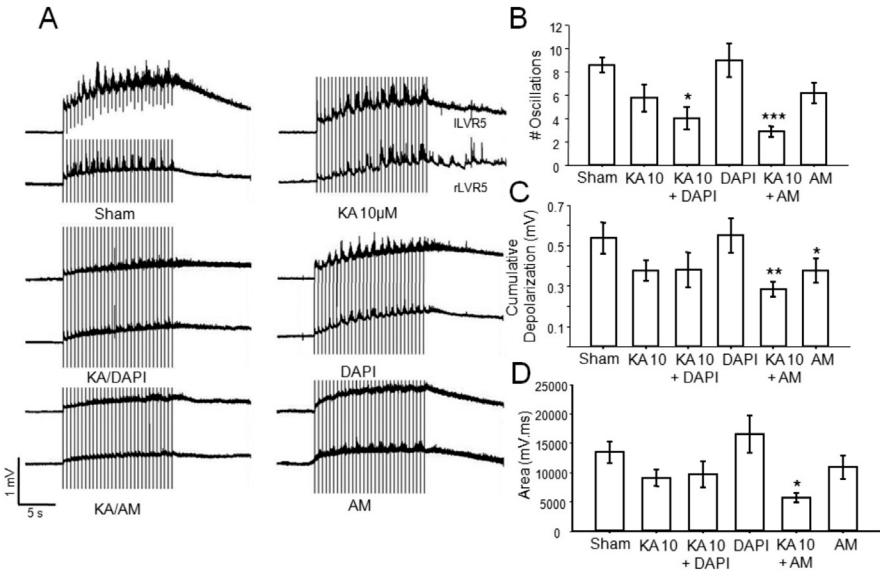

Fig. 7. Functional effect of ASIC inhibitors on mouse isolated spinal cord. (**A**) Examples of electrically evoked oscillatory patterns recorded from lumbar VRs 24 h after application of KA alone or followed by DAPI or amiloride. (**B**) Bar chart indicating the number of oscillations detected with sham, KA, KA/DAPI., DAPI, KA/amiloride or amiloride protocols. Note significant reduction in KA/DAPI and KA/amiloride responses (n = 11–16 spinal cords preparations; $^{*}p \leqslant 0.05$; $^{***}p \leqslant 0.001$, ANOVA, Tukey–Kramer). (**C**) Histograms showing cumulative depolarization amplitude for the above protocols; $^{*}p \leqslant 0.05$; $^{**}p \leqslant 0.005$, ANOVA, Fisher LSD. (**D**) Bar graph summarizing the area of DR evoked cumulative depolarization; $^{*}p \leqslant 0.05$, ANOVA, Tukey–Kramer.

Involvement of ASIC channels in the effect evoked by KA

In standard recording conditions DAPI had no effect on synaptic transmission or locomotor network rhythms while amiloride depressed polysynaptic activity. The latter phenomenon might be attributed to other actions by amiloride like inhibition of Cl^- transport, and of certain subtypes of Na^+ and K^+ channels (Leng et al., 2016). Although amiloride and its chemical derivatives are currently proposed as tools to develop ASIC channel blockers (Leng et al., 2016), it seems probable that the effects of amiloride on excitotoxicity could not be simply due to ASIC block. Nevertheless, in analogy to the effect of DAPI, one may posit that ASIC inhibition by DAPI or amiloride favoured excitotoxicity. Because the relatively modest acidification evoked by 10 μM KA had rather small effects on network function, it seems likely that the fall in extracellular pH evoked by KA was probably followed by reactive changes in intracellular

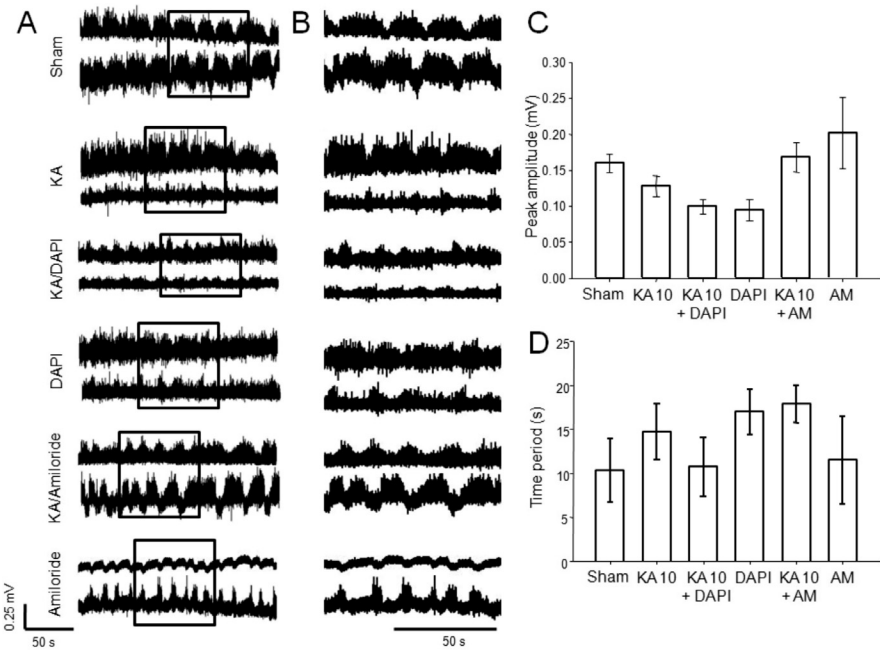

Fig. 8. NMDA and 5-HT evoked VR oscillations of mouse spinal cord. (A) Representative traces of oscillatory patterns evoked by excitatory chemicals applied with the protocols mentioned in Fig. 6. Traces are shown on a slow time scale on the left and records within boxed sections are also depicted on a faster time base on the right (B). (C) Histograms showing peak amplitude of the observed rhythms. Pooled data shown here are from spinal cords which produced at least 4 oscillations. Note there is no significant difference in the amplitude ($p = 0.14$, ANOVA) (D) Bar graphs indicating the rhythm periodicity. There is no significant change in between groups ($p = 0.49$, ANOVA, $n = 5–12$ spinal cords preparations).

pH as has been demonstrated in brain trauma and SCI (Huang et al., 2015b). Furthermore, early (and often overlooked) experiments had shown that moderate acidification can protect cortical or cerebellar neurons from excitotoxicity via block of NMDA receptor-mediated currents (Giffard et al., 1990; Andreeva et al., 1992) because H^+ is a strong modulator of the NMDA channel activity (Tang et al., 1990). In the present investigation ASIC inhibitors applied after KA substantially depressed network activities, especially those that required coherent oscillatory patterns. Indeed, when the ASIC inhibitors were applied after KA, the orderly recruitment of circuit elements was disrupted so that locomotor-network oscillations evoked by DR stimuli were significantly decreased. Conversely, there was much less disruption of locomotor rhythm when NMDA and 5-HT were bath applied to induce fictive locomotion. This discrepancy was due to the fact that, in the mammalian spinal cord, the ventral part of lumbar region itself can generate alternated rhythmic pattern even after ablating the dorsal horns (Kiehn and Kjaerulff, 1998; Ballerini et al., 1999) which are the areas where the strongest lesion by kainate is observed (Mazzone et al., 2010).

Mechanisms of delayed neurotoxicity by ASICs inhibitors

On the assumption that the operation of ASIC channels somehow raised the threshold for KA neurotoxicity, the question then arises how that would have been possible. Recent studies have indicated a physiological role of ASICs expressed by the central region of the lamprey spinal cord for detecting pH changes with a negative feedback to motor circuits resulting in suppression of locomotor activity (Jalalvand et al., 2016a,b). This implies that the spinal cord, at least of lower vertebrates, has a precise control system for sensing pH changes. In the mouse spinal cord an analogous system might rely on pH changes to deploy several effectors to contrast excitotoxicity at different times after the initial insult. While considering the relatively short time frame from the start of KA application, we would like to propose that ASIC activation might depress spike activity and, therefore, restrict the network excitation induced by KA (Vukicevic and Kellenberger, 2004), or that acidification may relieve the inhibitory interaction of ASIC channels with membrane K^+ channels, thereby favouring membrane potential repolarization (Petroff et al., 2008). At later times, KA-evoked stimulation and proliferation of neuroprecursors in the central region (Mazzone et al., 2013) might be mediated by upregulation of ASIC gene activity as observed in the present study. Furthermore, ASIC1a-mediated Ca^{2+} influx with consequent ERK 1/2 and Akt activity (Su et al., 2014) may upregulate Homer1 proteins that play an important role in synaptic plasticity of the spinal cord (Miletic et al., 2009) and are neuroprotective in traumatic brain injury (Luo et al., 2014). These possibilities should be investigated in future studies.

CONCLUSIONS

Our work proposes that moderate extracellular acidification might contribute to ASIC activation in turn likely to trigger cell processes to diminish excitability and neuronal loss with a relatively short delay. One might envisage a scenario where this process perhaps operates in concert with another mechanism, namely pH-mediated opening of leak K^+ channels that can also be activated pharmacologically by a neuroprotective volatile anesthetic (Shabbir et al., 2015b).

Our earlier results indicate that contrasting an intense excitotoxic insult may require intracellular processes like HSP70-dependent inhibition of non-apoptotic cell death (Shabbir et al., 2015a). Combinatorial strategies adopted by endogenous neuroprotective processes might be the reason why excitotoxic neuronal death in the rodent and human spinal cord is often limited to the minority of neurons (Mazzone et al., 2010) although the functional impact is suppression of locomotor-like output (Taccola et al., 2008).

CONFLICT OF INTERESTS

The authors declare no conflict of interest.

Acknowledgments—We thank Beatrice Pastore and Maria Eugenia Martin for the assistance with spinal cultures and mice genotyping. This study was supported by the Friuli Venezia Giulia Region (SPINAL project), Fundación para la Lucha contra las Enfermedades Neurológicas de la Infancia (FLENI), Consejo Nacional de Investigaciones Científicas y Técnicas (CONICET) and Regular Associate Scheme of the Abdus Salam International Centre for Theoretical Physics (ICTP).

REFERENCES

Alexander SPH, Mathie A, Peters JA (2011) Guide to receptors and channels (GRAC), 5th edition. Br J Pharmacol 164(Suppl 1): S1–S324.

Andreeva N, Khodorov B, Stelmashook E, Sokolova S, Cragoe E, Victorov I (1992) 5-(N-ethyl-N-isopropyl)amiloride and mild acidosis protect cultured cerebellar granule cells against glutamate-induced delayed neuronal death. Neuroscience 49:175–181.

Anwar MA, Al Shehabi TS, Eid AH (2016) Inflammogenesis of secondary spinal cord injury. Front Cell Neurosci:10.

Arun T, Tomassini V, Sbardella E, de Ruiter MB, Matthews L, Leite MI, Gelineau-Morel R, Cavey A, Vergo S, Craner M, Fugger L, Rovira A, Jenkinson M, Palace J (2013) Targeting ASIC1 in primary progressive multiple sclerosis: evidence of neuroprotection with amiloride. Brain 136:106–115.

Ballerini L, Galante M, Grandolfo M, Nistri A (1999) Generation of rhythmic patterns of activity by ventral interneurones in rat organotypic spinal slice culture. J Physiol 517:459–475.

Baraldi PG, Bovero A, Fruttarolo F, Preti D, Tabrizi MA, Pavani MG, Romagnoli R (2004) DNA minor groove binders as potential antitumor and antimicrobial agents. Med Res Rev 24:475–528.

Baranauskas G, Nistri A (1996) NMDA receptor-independent mechanisms responsible for the rate of rise of cumulative depolarization evoked by trains of dorsal root stimuli on rat spinal motoneurones. Brain Res 738:329–332.

Barbieri M, Nistri A (2001) Depression of windup of spinal neurons in the neonatal rat spinal cord in vitro by an NK3 tachykinin receptor antagonist. J Neurophysiol 85:1502–1511.

Baron A, Voilley N, Lazdunski M, Lingueglia E (2008) Acid sensing ion channels in dorsal spinal cord neurons. J Neurosci 28:1498–1508.

Beato M, Bracci E, Nistri A (1997) Contribution of NMDA and non-NMDA glutamate receptors to locomotor pattern generation in the neonatal rat spinal cord. Proc Roy Soc Biol Sci 264:877–884.

Borgens RB, Liu-Snyder P (2012) Understanding secondary injury. Q Rev Biol 87:89–127.

Boscardin E, Alijevic O, Hummler E, Frateschi S, Kellenberger S (2016) International union of basic and clinical pharmacology review acid-sensing ion channel and epithelial Na+ channel nomenclature review: IUPHAR Review. Br J Pharmacol. doi: 10.1111/bph.13533. [Epub ahead of print].

Brana C, Benham C, Sundstrom L (2002) A method for characterising cell death in vitro by combining propidium iodide staining with immunohistochemistry. Brain Res Protoc 10:109–114.

Chen X, Qiu L, Li M, Dürrnagel S, Orser BA, Xiong Z-G, MacDonald JF (2010) Diarylamidines: High potency inhibitors of acid-sensing ion channels. Neuropharmacology 58:1045–1053.

Chesler M (2003) Regulation and modulation of pH in the brain. Physiol Rev 83:1183–1221.

Chu X-P, Xiong Z-G (2012) Physiological and pathological functions of acid-sensing ion channels in the central nervous system. Curr Drug Targets 13:263–271.

Cifra A, Mazzone GL, Nani F, Nistri A, Mladinic M (2012) Postnatal developmental profile of neurons and glia in motor nuclei of the brainstem and spinal cord, and its comparison with organotypic slice cultures. Dev Neurobiol 72:1140–1160.

Deval E, Lingueglia E (2015) Acid-sensing Ion channels and nociception in the peripheral and central nervous systems. Neuropharmacology 94:49–57.

Dietz V (2010) Behavior of spinal neurons deprived of supraspinal input. Nat Rev Neurol 6:167–174.

Duan B, Wu L-J, Yu Y-Q, Ding Y, Jing L, Xu L, Chen J, Xu T-L (2007) Upregulation of acid-sensing ion channel ASIC1a in spinal dorsal horn neurons contributes to inflammatory pain hypersensitivity. J Neurosci 27:11139–11148.

Gahwiler BH (1981) Organotypic monolayer cultures of nervous tissue. J Neurosci Methods 4:329–342.

Giffard RG, Monyer H, Christine CW, Choi DW (1990) Acidosis reduces NMDA receptor activation, glutamate neurotoxicity, and oxygen-glucose deprivation neuronal injury in cortical cultures. Brain Res 506:339–342.

Gründer S, Pusch M (2015) Biophysical properties of acid-sensing ion channels (ASICs). Neuropharmacology 94:9–18.

Hnasko TS, Edwards RH (2012) Neurotransmitter co-release: mechanism and physiological role. Annu Rev Physiol 74:225–243.

Holzer P (2009) Acid-sensitive ion channels and receptors. Handb Exp Pharmacol 194:283–332.

Hu R, Duan B, Wang D, Yu Y, Li W, Luo H, Lu P, Lin J, Zhu G, Wan Q, Feng H (2011) Role of acid-sensing ion channel 1a in the secondary damage of traumatic spinal cord injury. Ann Surg 254:353–362.

Huang L, Zhao S, Lu W, Guan S, Zhu Y, Wang J-H (2015a) Acidosis-induced dysfunction of cortical GABAergic neurons through astrocyte-related excitotoxicity. PLoS ONE 10: e0140324.

Huang Y, Jiang N, Li J, Ji Y-H, Xiong Z-G, Zha X (2015b) Two aspects of ASIC function: synaptic plasticity and neuronal injury. Neuropharmacology 94:42–48.

Jalalvand E, Robertson B, Wallén P, Grillner S (2016a) Ciliated neurons lining the central canal sense both fluid movement and pH through ASIC3. Nat Commun 7:10002.

Jalalvand E, Robertson B, Tostivint H, Wallén P, Grillner S (2016b) The spinal cord has an intrinsic system for the control of pH. Curr Biol 26:1346–1351.

Kiehn O (2006) Locomotor circuits in the mammalian spinal cord. Annu Rev Neurosci 29:279–306.

Kiehn O (2016) Decoding the organization of spinal circuits that control locomotion. Nat Rev Neurosci 17:224–238.

Kiehn O, Kjaerulff O (1998) Distribution of central pattern generators for rhythmic motor outputs in the spinal cord of limbed vertebrates. Ann New York Acad Sci 860:110–129.

Kjaerulff O, Kiehn O (1996) Distribution of networks generating and coordinating locomotor activity in the neonatal rat spinal cord in vitro: a lesion study. J Neurosci 16:5777–5794.

Krishtal O (2003) The ASICs: signaling molecules? Modulators? Trends Neurosci 26:477–483.

Leng T-D, Si H-F, Li J, Yang T, Zhu M, Wang B, Simon RP, Xiong Z-G (2016) Amiloride analogs as ASIC1a inhibitors. CNS Neurosci Ther 22:468–476.

Li T, Yang Y, Canessa CM (2014) A method for activation of endogenous acid-sensing ion channel 1a (ASIC1a) in the nervous system with high spatial and temporal precision. J Biol Chem 289:15441–15448.

Llaudet E, Hatz S, Droniou M, Dale N (2005) Microelectrode biosensor for real-time measurement of ATP in biological tissue. Anal Chem 77:3267–3273.

Luo P, Chen T, Zhao Y, Zhang L, Yang Y, Liu W, Li S, Rao W, Dai S, Yang J, Fei Z (2014) Postsynaptic scaffold protein Homer 1a protects against traumatic brain injury via regulating group I metabotropic glutamate receptors. Cell Death Dis 5:e1174.

Ma L, Zhang X, Zhou M, Chen H (2012) Acid-sensitive TWIK and TASK two-pore domain potassium channels change ion selectivity and become permeable to sodium in extracellular acidification. J Biol Chem 287:37145–37153.

Marchetti C, Beato M, Nistri A (2001) Alternating rhythmic activity induced by dorsal root stimulation in the neonatal rat spinal cord in vitro. J Physiol (Lond) 530:105–112.
Mazzone GL, Margaryan G, Kuzhandaivel A, Nasrabady SE, Mladinic M, Nistri A (2010) Kainate-induced delayed onset of excitotoxicity with functional loss unrelated to the extent of neuronal damage in the in vitro spinal cord. Neuroscience 168:451–462.
Mazzone GL, Mladinic M, Nistri A (2013) Excitotoxic cell death induces delayed proliferation of endogenous neuroprogenitor cells in organotypic slice cultures of the rat spinal cord. Cell Death Dis 4:e902.
Mazzone GL, Nistri A (2011a) Effect of the PARP-1 inhibitor PJ 34 on excitotoxic damage evoked by kainate on rat spinal cord organotypic slices. Cell Mol Neurobiol 31:469–478.
Mazzone GL, Nistri A (2011b) Electrochemical detection of endogenous glutamate release from rat spinal cord organotypic slices as a real-time method to monitor excitotoxicity. J Neurosci Meth 197:128–132.
Mazzone GL, Rigato I, Ostrow JD, Tiribelli C (2009) Bilirubin effect on endothelial adhesion molecules expression is mediated by the NF-kappaB signaling pathway. Biosci Trends 3:151–157.
Miletic G, Driver AM, Miyabe-Nishiwaki T, Miletic V (2009) Early changes in Homer1 proteinsin the spinal dorsal horn are associated with loose ligation of the rat sciatic nerve. Anesth Analg 109:2000–2007.
Mitra P, Brownstone RM (2012) An in vitro spinal cord slice preparation for recording from lumbar motoneurons of the adult mouse. J Neurophysiol 107:728–741.
Osmakov DI, Andreev YA, Kozlov SA (2014) Acid-sensing ion channels and their modulators. Biochemistry (Moscow) 79:1528–1545.
Oyinbo CA (2011) Secondary injury mechanisms in traumatic spinal cord injury: a nugget of this multiply cascade. Acta Neurobiol Exp (Wars) 71:281–299.
Park E, Velumian AA, Fehlings MG (2004) The role of excitotoxicity in secondary mechanisms of spinal cord injury: a review with an emphasis on the implications for white matter degeneration. J Neurotrauma 21:754–774.
Petroff EY, Price MP, Snitsarev V, Gong H, Korovkina V, Abboud FM, Welsh MJ (2008) Acid-sensing ion channels interact with and inhibit BK K+ channels. Proc Natl Acad Sci USA 105:3140–3144.
Pfaffl MW (2001) A new mathematical model for relative quantification in real-time RT-PCR. Nucleic Acids Res 29:e45.
Price MP, McIlwrath SL, Xie J, Cheng C, Qiao J, Tarr DE, Sluka KA, Brennan TJ, Lewin GR, Welsh MJ (2001) The DRASIC cation channel contributes to the detection of cutaneous touch and acid stimuli in mice. Neuron 32:1071–1083.
Quintana P, Soto D, Poirot O, Zonouzi M, Kellenberger S, Muller D, Chrast R, Cull-Candy SG (2015) Acid-sensing ion channel 1a drives AMPA receptor plasticity following ischaemia and acidosis in hippocampal CA1 neurons. J Physiol (Lond) 593:4373–4386.
Robinson DL, Hermans A, Seipel AT, Wightman RM (2008) Monitoring rapid chemical communication in the brain. Chem Rev 108:2554–2584.
Ruffin VA, Salameh AI, Boron WF, Parker MD (2014) Intracellular pH regulation by acid-base transporters in mammalian neurons. Front Physiol 5:43.
Shabbir A, Bianchetti E, Cargonja R, Petrovic A, Mladinic M, Pilipović K, Nistri A (2015a) Role of HSP70 in motoneuron survival after excitotoxic stress in a rat spinal cord injury model in vitro. Eur J Neurosci 42:3054–3065.
Shabbir A, Bianchetti E, Nistri A (2015b) The volatile anesthetic methoxyflurane protects motoneurons against excitotoxicity in an in vitro model of rat spinal cord injury. Neuroscience 285:269–280.
Sinning A, Hübner CA (2013) Minireview: pH and synaptic transmission. FEBS Lett 587:1923–1928.
Sivilotti LG, Thompson SW, Woolf CJ (1993) Rate of rise of the cumulative depolarization evoked by repetitive stimulation of small-caliber afferents is a predictor of action potential windup in rat spinal neurons in vitro. J Neurophysiol 69:1621–1631.
Su J-J, Pan H, Zhou H-G, Tang Y-P, Dong Q, Liu J-R (2014) Acid-sensing ion channels activation and hypoxia upregulate Homer1a expression. CNS Neurosci Ther 20:264–274.
Swain SM, Parameswaran S, Sahu G, Verma RS, Bera AK (2012) Proton-gated ion channels in mouse bone marrow stromal cells. Stem Cell Research 9:59–68.
Taccola G, Margaryan G, Mladinic M, Nistri A (2008) Kainate and metabolic perturbation mimicking spinal injury differentially contribute to early damage of locomotor networks in the in vitro neonatal rat spinal cord. Neuroscience 155:538–555.
Tang CM, Dichter M, Morad M (1990) Modulation of the N-methyl-D-aspartate channel by extracellular H^+. Proc Natl Acad Sci USA 87:6445–6449.
Vukicevic M, Kellenberger S (2004) Modulatory effects of acid-sensing ion channels on action potential generation in hippocampal neurons. Am J Physiol – Cell Physiol 287: C682–C690.
Wemmie JA, Chen J, Askwith CC, Hruska-Hageman AM, Price MP, Nolan BC, Yoder PG, Lamani E, Hoshi T, Freeman Jr JH, Welsh MJ (2002) The acid-activated ion channel ASIC contributes to synaptic plasticity, learning, and memory. Neuron 34:463–477.
Xiong Z-G, Zhu X-M, Chu X-P, Minami M, Hey J, Wei W-L, MacDonald JF, Wemmie JA, Price MP, Welsh MJ, Simon RP (2004) Neuroprotection in ischemia: blocking calcium-permeable acid-sensing ion channels. Cell 118:687–698.
Yang L, Palmer LG (2014) Ion conduction and selectivity in acid-sensing ion channel 1. J Gen Physiol 144:245–255.
Zhong G, Shevtsova NA, Rybak IA, Harris-Warrick RM (2012) Neuronal activity in the isolated mouse spinal cord during spontaneous deletions in fictive locomotion: insights into locomotor central pattern generator organization. J Physiol (Lond) 590:4735–4759.

(Received 31 August 2016, Accepted 4 December 2016)
(Available online 19 December 2016)